RESEARCH ARTICLE

Towards impedance-based temperature estimation for Li-ion battery packs

Henrik Beelen[1] | Kartik Mundaragi Shivakumar[1] | Luc Raijmakers[2] | M.C.F. Donkers[1] | Henk Jan Bergveld[1,3]

[1]Department of Electrical Engineering, Eindhoven University of Technology, Eindhoven, Netherlands

[2]Department of Fundamental Electrochemistry, Forschungszentrum Jülich, Germany

[3]NXP Semiconductors, Eindhoven, Netherlands

Correspondence
Henrik Beelen, Control Systems Group, Department of Electrical Engineering, Eindhoven University of Technology, PO Box 513, 5600 MB Eindhoven, Netherlands.
Email: h.p.g.j.beelen@tue.nl

Summary

In order to meet the required power and energy demand of battery-powered applications, battery packs are constructed from a multitude of battery cells. For safety and control purposes, an accurate estimate of the temperature of each battery cell is of vital importance. Using electrochemical impedance spectroscopy (EIS), the battery temperature can be inferred from the impedance. However, performing EIS measurements simultaneously at the same frequency on each cell in a battery pack introduces crosstalk interference in surrounding cells, which may cause EIS measurements in battery packs to be inaccurate. Also, currents flowing through the pack interfere with impedance measurements on the cell level. In this paper, we propose, analyse, and validate a method for estimating the battery temperature in a battery pack in the presence of these disturbances. First, we extend an existing and effective estimation framework for impedance-based temperature estimation towards estimating the temperature of each cell in a pack in the presence of crosstalk and (dis)charge currents. Second, the proposed method is analysed and validated on a two-cell battery pack, which is the first step towards development of this method for a full-size battery pack. Monte Carlo simulations are used to find suitable measurement settings that yield small estimation errors and it is demonstrated experimentally that, over a range of temperatures, the method yields an accuracy of $\pm 1^\circ$C in terms of bias, in the presence of both disturbances.

KEYWORDS

battery packs, battery temperature, electrochemical impedance spectroscopy, lithium-ion batteries

NOVELTY STATEMENT

Monitoring battery temperature is important for Li-ion battery management and can be done accurately and fast using impedance-based temperature estimation. The existing literature predominantly focuses on single battery cells, often under laboratory conditions. We present an important extension to impedance-based temperature estimation by considering the challenges that arise when the

method is employed in multicell battery packs as present in many practical applications: interference from (dis)charge currents and crosstalk induced by inductive coupling during simultaneous impedance measurements of the cells.

1 | INTRODUCTION

Lithium-ion batteries are often used to power, eg, (hybrid) electric vehicles. To ensure safe use of the battery and to warrant a certain lifetime, battery temperature plays a vital role. Therefore, one of the purposes of a battery management system (BMS) is to monitor temperature and to keep it within a specified range.[1,2] For example, high battery temperatures can induce thermal runaway, which may cause fire or explosions[3] and accelerate ageing of the battery, thus reducing lifetime and performance.[2] Various temperature indication methods exist for Li-ion batteries.[4] While the measured surface temperature is usually assumed to be close to the (average) internal temperature of the battery, the internal temperature may differ significantly from the surface temperature, especially under (heavy) load conditions. Under these conditions, substantial heat generation can occur internally in the battery cell. This may lead to the development of thermal gradients, in which case the measured surface temperate could (significantly) underestimate the maximum (internal) temperature of the battery cell; see, eg, Raijmakers et al[4] and references therein. For battery safety, accurate information of the internal temperature is important for early detection of thermal runaway. Considering the recent trend of battery pack supervision on the cell level, instead of measuring the surface temperature directly with external temperature sensors, the (average) internal temperature can be estimated using online electrochemical impedance spectroscopy (EIS)[5,6] by inferring a temperature relation between the electrochemical battery impedance and the battery temperature.[7-16] Using impedance-based temperature estimation is a promising technique as it may provide faster and more accurate information on the (average) internal temperature of a battery cell. Although in some cases the EIS measurements may increase the hardware cost of battery management, in applications where batteries are monitored at the cell level, the EIS measurement can be performed with (minor adjustments to) the electronics that are already present at little or no increase in cost. More precisely, the stimulus for performing EIS measurements in this study is generated by reusing the passive-balancing hardware already present.[17]

A number of methods for impedance-based temperature estimation exist. For instance, Schmidt et al[10] relate the real part of the impedance at a fixed frequency to the battery temperature. This is also done by Richardson

et al.[18] However, they also use a thermal-impedance model (eg, the heat equation for heat conduction in a cylinder) combined with measurements of the surface temperature. In more recent work, this thermal-impedance model only takes the EIS-based temperature estimate as an input.[12] For the sake of comparing estimation methods in terms of their impedance-based temperature estimation, the thermal-impedance model is not taken into account. Contrary to the aforementioned methods, Spinner et al[15] infer a temperature relation from the imaginary part of the impedance at a fixed frequency rather than from the real part of the impedance. Instead of relating temperature to either the real or imaginary part of the impedance, Srinivasan,[11] who expands on previous work,[19] infers a relation from the phase shift of the impedance. It should be noted that the aforementioned methods do not necessarily choose the same frequency. Raijmakers et al[8] do not employ a fixed frequency but define the so-called zero-intercept frequency, ie, the frequency for which the imaginary part of the impedance is zero. This implies that a relation based on the imaginary part of the impedance is used. Finally, Beelen et al[7] have developed a general framework for comparison, analysis, and synthesis of methods for impedance-based temperature estimation in which all existing methods can be considered as special cases of this general framework.

Most of the aforementioned research on using EIS for temperature estimation demonstrates this functionality on the single-cell level, often under laboratory conditions. In order to provide more power and energy for certain applications, single cells need to be connected in series and/or parallel to form a battery pack. To allow individual cells to be monitored, it is of interest to understand how EIS measurements on single cells are affected by the measurement artefacts present in battery packs, namely, (dis)charge currents and crosstalk interference, ie, interference induced by simultaneously performing EIS (at the same frequency) on several cells in a battery pack. Although crosstalk interference can easily be avoided by measuring the impedance of the battery cells one by one, ie, not measuring simultaneously, this will lead to relatively high sample times for the temperature estimates. Therefore, this is not suitable for real-time monitoring of the (average) internal temperature, which is of paramount importance for safety of the battery cell (eg, early detection of thermal runaway). Therefore, if we accept the problem of crosstalk and are able to find a solution for this problem, impedance-based temperature estimation would be a suitable method for application in battery packs. Both of the aforementioned artefacts are known to influence the EIS measurements, as was shown for (dis)charge currents by Raijmakers et al[9] and for crosstalk interference.[20] However, a solution on how to deal the combination of

these two artefacts and how to conduct impedance-based temperature estimation for battery packs accurately has not yet been presented in the existing literature.

In this paper, we will study impedance-based temperature estimation in the combined presence of (dis)charge currents and crosstalk interference induced by simultaneous impedance measurements in cells. To the best of the authors' knowledge, there have not yet been any studies that have investigated the applicability of impedance-based temperature estimation to battery packs since the existing literature focuses predominantly on impedance-based temperature estimation at the cell level. Therefore, the goal of this paper is to develop and present a solid proof of concept which shows that impedance-based temperature estimation can be extended towards battery packs. However, as we will take the first steps towards the extension of the method, more research will be needed to further develop and extensively validate the method in order to advance it to a more mature state.

As a first contribution of the paper, we will focus on modelling crosstalk interference and (dis)charge currents in order to incorporate these artefacts in the framework for impedance-based temperature estimation.[7] It is shown that crosstalk depends neither on temperature nor on battery state-of-charge (SoC), which has not been investigated by Raijmakers et al.[20] Subsequently, we will show how the disturbance caused by the measured time-domain (dis)charge currents can be modelled as a frequency-domain disturbance on the measured impedance. This will be done by using both a deterministic and a stochastic modelling approach. Then, we will show how these models can be incorporated in the temperature estimation framework presented in our previous work.[7] More precisely, the crosstalk model can be used to compensate for the effect of crosstalk on the temperature estimation. However, since it is not possible to measure the (dis)charge current synchronously with the impedance measurements with the electronics used in this study,[1] the model of the (dis)charge current cannot be used to compensate for the effect of the (dis)charge current. Therefore, the latter model will be used purely for analysis purposes so as to investigate the (deteriorating) effect of this artefact on the temperature estimation. The topic of synchronously measuring the battery impedance with the (dis)charge current can be seen as an important next step in the development of methods for impedance-based temperature estimation in battery packs.

Second, we will use the so-called extended temperature estimation framework to design the optimal (in the mean-square-error sense) temperature estimation method. In the design process, the excitation frequency used in EIS and the weighting between real and imaginary part of the impedance can be chosen so as to arrive at the lowest mean-square estimation error (MSE). We will analyse the consequence of these design choices on the accuracy of the method using a Monte Carlo simulation study in the presence of crosstalk, (dis)charge currents, and in the presence of both artefacts simultaneously. All of these cases will lead to a different optimal impedance-based temperature estimation procedure. We will demonstrate the most accurate impedance-based temperature estimation method experimentally on a two-cell battery pack, which can be interpreted as the first step of developing this method towards application on a full-size battery pack.

The outline of this paper is as follows. The general concept of impedance-based temperature estimation in battery cells or battery packs is introduced in Section 2. Subsequently, in Sections 3 and 4, crosstalk interference and (dis)charge currents, respectively, will be investigated and modelled. The extended estimation framework, based on the framework presented by Beelen et al,[7] is then derived in Section 5, using the modelled crosstalk and (dis)charge current interference. In Section 6, the extended temperature estimation framework is used in a Monte Carlo simulation study to analyse the effect of the design choices in terms of the accuracy of temperature estimation. An optimal impedance-based temperature estimation method will be derived from this analysis and validated experimentally in Section 7. Finally, conclusions are drawn in Section 8.

2 | IMPEDANCE-BASED TEMPERATURE ESTIMATION

In this section, first, we will briefly summarise the framework for impedance-based temperature estimation[7] and introduce a general impedance model for the case of arranging multiple battery cells into a battery pack, which can be used in combination with the aforementioned framework. Furthermore, the experimental setup that is used for modelling, analysis, and validation will be presented.

2.1 | Impedance-based temperature estimation framework

The concept of impedance-based temperature estimation and the general estimation framework for comparison, accuracy analysis, and synthesis of impedance-based estimation methods have been introduced in our previous work[7] and can be summarised as follows.

The battery impedance Z can be interpreted as the battery frequency response, where the battery takes a sinusoidal voltage or current input with frequency f, and produces a sinusoidal current or voltage output, respectively, with the same frequency. The ratio between input and output can be described as a (complex) impedance

$$Z(f) = \frac{V(f)}{I(f)}, \qquad (1)$$

where the magnitude of the excitation signal should be sufficiently small in order to guarantee local linearity of the system yet not too small to prevent a poor signal-to-noise ratio (SNR). The technique of obtaining the frequency response of the battery is known as EIS and is widely used for gathering information about batteries.[5,21-24] In this study, EIS measurements have been conducted in galvanostatic mode by superimposing a sinusoidal current of a single frequency f with an amplitude of $100\sqrt{2}$ mA on the load current of the battery (whether or not a load current is present). The single-frequency approach is taken in this paper because of the limitations of the (prototype) measurement device. However, methods for conducting EIS measurements with a certain frequency band also exist; see, eg, Ranieri et al,[24] where a pseudorandom binary sequence of a certain bandwidth is used to excite the battery.

The modelling concept that we follow can be described as follows. The true battery impedance can be denoted by Z and can be interpreted as a function $Z : \mathbb{R}^3 \to \mathbb{C}$ that depends on excitation frequency f, temperature T, SoC, and possibly other effects not considered in this study, such as battery ageing.[25] Although it is important to investigate and take into account the effect of ageing on the battery impedance and the corresponding temperature estimates,[8,26] this paper focuses on two issues directly related to extending the method of impedance-based temperature estimation to battery packs. Investigating the ageing phenomenon can be seen as a separate valuable next step for future research. A model of the impedance Z can be denoted by $\hat{Z}$. It should be noted that the model $\hat{Z}$ is not based on modelling approaches such as first principles modelling or equivalent-circuit modelling[27,28] as this paper focuses on the (temperature) estimation problem and not on battery modelling. Instead, the model $\hat{Z}$ will be a *static* model based on a lookup table for which we will assume that $\hat{Z}$ only depends on f, T, and SoC. Moreover, the signal analysis techniques that are needed to obtain Z from (1) are not investigated in this paper. Incorporating the dependency of the impedance on f, T, and SoC results in the lookup table mapping $\hat{Z} : \mathbb{R}^3 \to \mathbb{C}$. More precisely, the model $\hat{Z}$ will consist of a three-dimensional lookup table that takes f, T, and SoC as inputs for the lookup action. Consequently, this means that

the modelled impedance $\hat{Z}$ is only available for the finite range of f, T, and SoC and the finite number of grid points of f, T, and SoC. The range can be chosen such that it covers the operational space of the battery. For values of f, T, and SoC in between the (measured) grid points, the modelled impedance $\hat{Z}$ can be obtained by using interpolation.

In order to construct the battery model $\hat{Z}$ (ie, filling the lookup table at certain grid points), the battery impedance needs to be measured at the selected grid points. Since the measurement device used in this paper introduces additive measurement noise $v \in \mathbb{C}$ to the measured impedance, the measured battery impedance can be interpreted as the true impedance Z with additive noise, ie,

$$Z^{\mathrm{meas}} = Z(f, T, \mathrm{SoC}) + v, \qquad (2)$$

where v is complex-valued zero-mean Gaussian noise. Subsequently, the lookup table $\hat{Z}$ can be constructed as follows. First, we assume that, by taking a sufficient number of measurements at every grid point, the average value of the additive noise will approach zero. Assuming that SoC information is available, eg, through SoC estimation, the model $\hat{Z}$ will be a three-dimensional lookup table (ie, f, T, and SoC as inputs) and can be constructed by

$$\hat{Z}(f_r, T_r, \mathrm{SoC}_r) = \frac{1}{L} \sum_{i=1}^{L} Z(f_r, T_r, \mathrm{SoC}_r) + v_i, \qquad (3)$$

where $L \in \mathbb{N}$ is the number of measurements taken per grid point. The frequency, temperature, and SoC grid points f_r, T_r, and SoC_r, respectively, need to be selected on the basis of the desired range of validity of the model $\hat{Z}$. Now, the model $\hat{Z}(f_r, T_r, \mathrm{SoC}_r)$ can be considered as a lookup table at the selected grid points. As mentioned previously, values in between the grid points can be obtained by interpolation, resulting in a battery model without grid-point indices $\hat{Z}(f, T, \mathrm{SoC})$ (ie, a lookup table model with built-in interpolation function).

To estimate the battery temperature on the basis of the modelled battery impedance $\hat{Z}$ and the measured battery impedance Z^{meas}, a nonlinear least-squares estimator has been developed in a previous study,[7] which is given by

$$\hat{T}(f, \alpha, Z^{\mathrm{meas}}, \mathrm{SoC}) = \arg\min_{T} \alpha \bar{Z}_1^2(f, T, Z^{\mathrm{meas}}, \mathrm{SoC})$$
$$+ (1 - \alpha)\bar{Z}_2^2(f, T, Z^{\mathrm{meas}}, \mathrm{SoC}), \qquad (4)$$

where f is the excitation frequency, Z^{meas} is the measured battery impedance obtained through EIS, and $\alpha \in [0, 1]$ denotes a selector variable. In Cartesian coordinates, $\bar{Z}_1$ and $\bar{Z}_2$ are given by

$$\bar{Z}_1(f,T,Z^{\text{meas}},\text{SoC}) = \text{Re}(\hat{Z}(f,T,\text{SoC}) - Z^{\text{meas}}), \quad (5a)$$

$$\bar{Z}_2(f,T,Z^{\text{meas}},\text{SoC}) = \text{Im}(\hat{Z}(f,T,\text{SoC}) - Z^{\text{meas}}). \quad (5b)$$

In (4), the real and imaginary parts of a complex number, eg, $Z = a + jb$, where $a, b \in \mathbb{R}$ and j satisfies $j^2 = -1$, are denoted by $\text{Re}(Z) = a$ and $\text{Im}(Z) = b$. For ease of exposition, only $\text{Re}(Z)$ and $\text{Im}(Z)$ are considered in this paper by $\bar{Z}_1$ and $\bar{Z}_2$, respectively, although other choices are possible.[7] In (4), taking $\alpha = 1$ can be interpreted as using only $\text{Re}(Z)$ to estimate the temperature and taking $\alpha = 0$ can be interpreted as using only $\text{Im}(Z)$ to estimate the temperature. Taking $0 \le \alpha \le 1$ will lead to a temperature estimate that is based on both $\text{Re}(Z)$ and $\text{Im}(Z)$. In this paper, a single impedance measurement will be used to estimate the temperature with the estimator in (4). This takes approximately 1 second. Of course, multiple impedance measurements (possibly at different frequencies) can be used in (4), which might yield a smaller estimation error since variations are averaged.[7] However, for ease of exposition and because of limitations imposed by the measurement device that is used in the experimental demonstration, we will use a single impedance measurement in this paper.

The framework for temperature estimation given by (4) is based on the impedance Z of a single battery cell, ie, $Z \in \mathbb{C}$ is a complex scalar. In case a battery pack of N cells in series is considered, as schematically depicted in Figure 1, the impedance Z is a frequency-response matrix that satisfies

$$\begin{bmatrix} V_1(f) \\ \vdots \\ V_N(f) \end{bmatrix} = \underbrace{\begin{bmatrix} Z_{11}(f,T,\text{SoC}) & \cdots & Z_{1N}(f,T,\text{SoC}) \\ \vdots & \ddots & \vdots \\ Z_{N1}(f,T,\text{SoC}) & \cdots & Z_{NN}(f,T,\text{SoC}) \end{bmatrix}}_{= Z(f,T,\text{SoC})} \begin{bmatrix} I_1(f) + D(f) \\ \vdots \\ I_N(f) + D(f) \end{bmatrix},$$
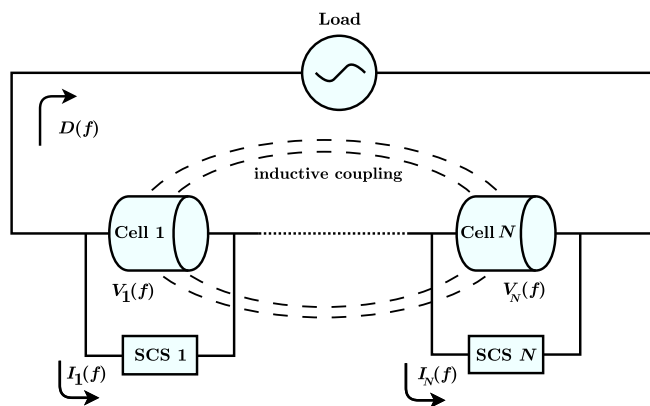
$$(6)$$

FIGURE 1 Diagram showing the currents and voltages in an N-cell battery pack, subject to electrochemical impedance spectroscopy (EIS) measurements per cell with the single-cell supervisor (SCS)

where $V_n(f)$ and $I_n(f)$, $n \in \{1, ..., N\}$ are the output voltages and input currents, respectively, of cell n and $Z_{mn}(f)$ are the frequency-response functions from cell n to cell m. The diagonal terms in Z represent the cell impedances as used in the previous study,[7] and the off-diagonal terms represent the crosstalk impedances from cell to cell that are caused by the inductive coupling between cells; see Raijmakers et al.[20] The term $D(f)$ represents the disturbance induced by (dis)charging the battery. In this paper, we assume that the battery pack consists of N cells, which are connected in series and placed adjacent to one another. Therefore, the same current $D(f)$ flows through each cell in the battery pack as shown in Figure 1. However, the methodology in this paper is not limited to series connections; it can also be used for any pack topology with parallel and/or series connections. In case of a parallel connection, $D(f)$ will be divided over the parallel branches of the battery pack. Consequently, instead of the entire (dis)charge current $D(f)$ flowing through the battery cells (and disturbing the impedance measurements), the pack current $D(f)$, divided by the number of parallel branches, will flow through the parallel-connected cells.

To assess the quality of a set of the temperature estimates $\{\hat{T}_i\}_{i=1}^k$ with respect to the actual temperature T, we will employ the notion of (sample) MSE given by $\text{MSE}(\hat{T}) = \frac{1}{k}\sum_{i=1}^k (\hat{T}_i - T)^2$. Furthermore, we will express the estimation quality in terms of the (sample) bias $b(\hat{T}, T)$ and the (sample) variance $\text{Var}(\hat{T})$ of the estimate, given by

$$b(\hat{T}) = M_k(\hat{T}) - T \quad \text{and} \quad \text{Var}(\hat{T}) = \frac{1}{k}\sum_{i=1}^k (\hat{T}_i - M_k(\hat{T}))^2, \quad (7)$$

where $M_k(\hat{T}) = \frac{1}{k}\sum_{i=1}^k \hat{T}_i$ is the sample mean of $\hat{T}$. Note that the (sample) SD $\sigma(\hat{T})$ satisfies $\sigma^2(\hat{T}) = \text{Var}(\hat{T})$. Therefore, MSE can be written as the sum of the variance and the squared bias of the estimator[29] as

$$\text{MSE}(\hat{T}) = \text{Var}(\hat{T}) + (b(\hat{T}))^2. \quad (8)$$

2.2 | Experimental setup

The experimental setup used in this paper is shown in Figure 2A. The setup consists of two rectangular prismatic nickel-manganese-cobalt (NMC) Li-ion cells, where the cells are closely matched in terms of capacity (ie, 23.26 Ah for cell 1 and 23.34 Ah for cell 2) and where each cell is connected to a single-cell supervisor (SCS) designed by NXP Semiconductors. The SCS draws a

sinusoidal current $I(f)$ with a DC component of -300 mA and an amplitude of $100\sqrt{2}$ mA (with a specified frequency f) from the cell and subsequently measures the induced voltage $V(f)$. Subsequently, the impedance of cell n is obtained by using $Z_n(f) = V_n(f)/I_n(f)$ with $n \in \{1, 2\}$.[2] This implies that the SCS of cell 1 will draw a current $I_1(f)$ and measure the voltage $V_1(f)$, whereas the SCS of cell 2 will draw a current $I_2(f)$ and measure the voltage $V_2(f)$. It should be noted that the SCS uses a single-frequency sinusoidal current as an excitation signal for the impedance measurements. The measurement frequency can be selected by the user; however, the amplitude and measurement time of the excitation signal are fixed. Moreover, note that the SCS is a passive measurement device, ie, the sinusoidal excitation signal is generated by switching a resistor in parallel with the battery cell using a pulse-density–modulated switching signal of a sine wave.[9,17] In order to obtain a sine wave perturbation using the passive circuit, the aforementioned DC component is needed. Consequently, the nonzero DC component of the excitation signal of the SCS causes a slight discharge of the cell under test. Note that this DC component would not be needed if an active current is used to generate the current perturbation for the impedance measurements (and consequently, there will be no discharge of the cell during the measurements). However, the reason for using the passive circuit is that it was possible to reuse the passive balancing electronics already present on the chip, ie, no additional hardware was needed. Consequently, adding the functionality of impedance measurements does not increase the cost of the chip. Moreover, using the passive approach with the DC component also yields useful results in terms of impedance measurements.

The accuracy of the SCS measurements can be characterised by the SDs σ_{Re} and σ_{Im} of the real and imaginary part of the impedance measurements, respectively. In

Figure 2B, the SDs of the impedance measurements are depicted as a function of frequency for the real and imaginary part of Z in blue and red, respectively. Note that this SD is a property of the measurement device, eg, Figure 2B shows that at $f = 1000$ Hz, the total impedance can be measured with $\sigma = \pm 14$ μΩ. When analysing the accuracy of impedance-based temperature estimation, this SD should be taken into account. In our previous study,[7] this has been done by means of the simplified assumption of a frequency-independent SD of $\sigma = \pm 14 \mu\Omega$, based on the spread of the impedance measurements. However, a frequency-dependent analysis (with averaging over T and SoC) of the measurement points results in the frequency-dependent SD as shown in Figure 2B, which will be used in this paper. It should be noted that a larger SD on the measured impedance does not necessarily imply a larger SD on the estimated temperature, since this depends on
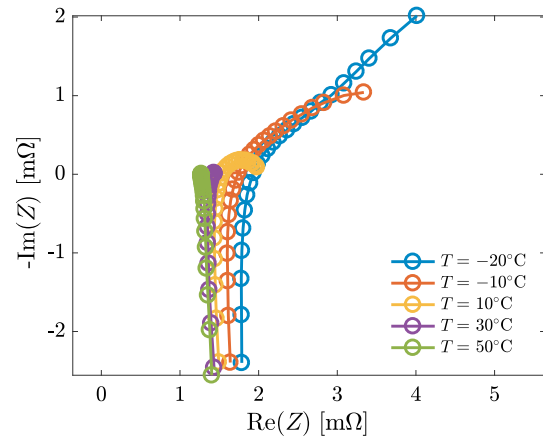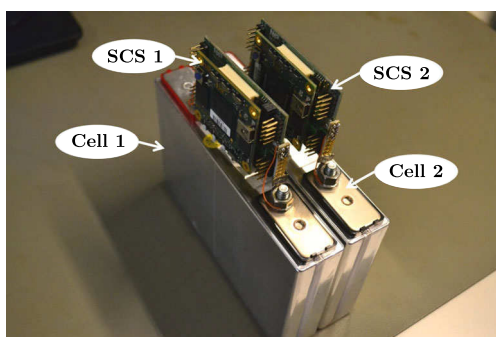

FIGURE 3 Nyquist plot of battery impedance Z_{11} of cell 1 at SoC = 60% for $f = 10$ Hz to $f = 5$ kHz. SoC, state-of-charge [Colour figure can be viewed at wileyonlinelibrary.com]

(A) Two-cell setup used for impedance measurements.
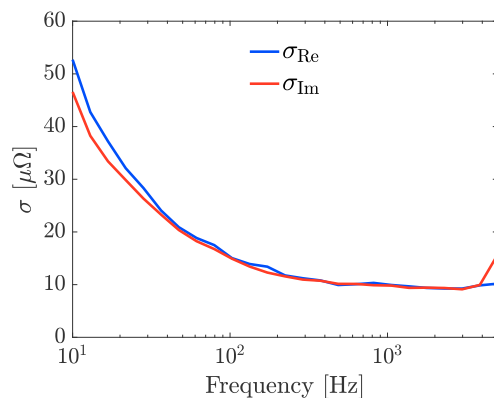
(B) Standard deviation of the measured battery impedance as a function of frequency f.

FIGURE 2 Experimental setup. (A) Two-cell setup used for impedance measurements. (B) SD of the measured battery impedance as a function of frequency f [Colour figure can be viewed at wileyonlinelibrary.com]

the sensitivity of the battery impedance with respect to temperature at a certain frequency.[7]

In this paper, the temperature estimation is always performed while the pack is under thermal equilibrium (ie, no evolution of temperature during impedance measurements) since it is necessary to know the actual battery temperature T in order to calculate the MSE of temperature estimation and to perform modelling experiments. However, impedance-based temperature estimation can be used when temperature gradients are present in the battery cell.[9,12,16] For temperature estimation measurements, the two cells are kept inside a Vötsch VT4002 temperature chamber to ensure that both cells are at a controlled temperature and that no temperature gradients are formed in the pack. In order to analyse the effect of (dis)charge currents on temperature estimation, a KEPCO BOP 20-20 M bipolar operational power supply and amplifier is used to generate the actual (dis)charge currents in the range [−20A, 20A]. Using the experimental setup, the temperature dependency of the battery impedance can be characterised, as shown in Figure 3, where the Nyquist plot of cell 1 is depicted for different temperatures and frequencies at SoC = 60%.

Finally, it is important to note that the two-cell setup in Figure 2A is used in this paper to develop a proof of concept for the extension of impedance-based temperature estimation towards battery packs. On the basis of the results presented in this paper, the next steps in research and validation (eg, using larger size battery packs) can be taken to develop the method to a more mature state.

3 | CROSSTALK

In this section, we will develop a model for crosstalk in battery packs. The existence of crosstalk was first shown by Raijmakers et al,[20] and we will briefly summarise these results. Then, as an extension to the study by Raijmakers et al,[20] the influence of SoC and T on crosstalk behaviour is investigated.

3.1 | Background on crosstalk behaviour

To show the influence of crosstalk on EIS measurements, let us consider the setup in Figure 2A, when a current of the same frequency f is drawn from both cells simultaneously and when both cells are at the same temperature T and SoC. In this case, an offset is observed in the measured impedance, when compared with the standalone impedance of each cell at the same frequency.[20] This offset is caused by the fact that the "perceived impedance" $Z_2^\star$ from $I_2(f)$ to $V_2(f)$, ie, $V_2(f) = Z_2^\star(f)I_2(f)$, is given by
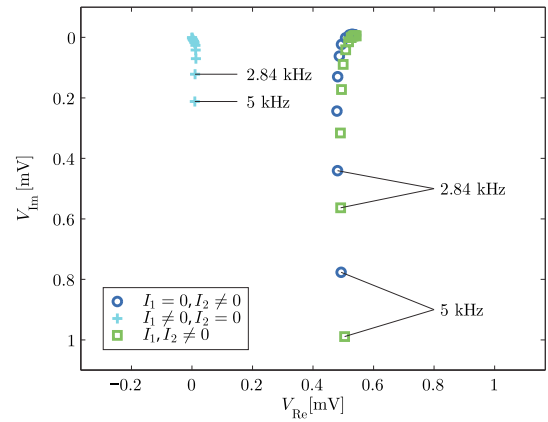

FIGURE 4 Example of the offset in measured voltage of cell 2, induced by crosstalk interference from cell 1 at multiple frequencies and in three different cases. Adjusted from Raijmakers et al[20] [Colour figure can be viewed at wileyonlinelibrary.com]

$$Z_2^\star(f) = Z_{22}(f) + Z_{21}(f)\frac{I_1(f)}{I_2(f)}, \quad (9)$$

which is not equal to the actual impedance $Z_{22}(f)$ when $I_1(f) \neq 0$.

This effect is visible in Figure 4, where the measured cell voltage for cell 2, ie, $V_2(f)$, is shown for multiple frequencies and for three different measurement conditions. Namely, the dark-blue circles depict the measured $V_2(f)$ in the absence of crosstalk interference from cell 1, ie, $I_2(f) \neq 0$ while $I_1(f) = 0$. The cyan pluses in Figure 4 depict $V_2(f)$ for the case where an AC current $I_1(f)$ has been drawn from cell 1, while $I_2(f) = 0$. Since the measured voltage $V_2(f) \neq 0$, this indicates that crosstalk between the two cells is present. Finally, the green squares in Figure 4 depict the measured voltage $V_2(f)$ for the case where an AC current has been drawn from both cells simultaneously, ie, $I_1(f) \neq 0$ and $I_2(f) \neq 0$. This measurement, which is influenced by crosstalk, differs considerably from the measurement without crosstalk (ie, the dark-blue circles). This effect is more pronounced for higher frequencies as is explicitly indicated in Figure 4 for frequencies of 2.84 and 5 kHz. This suggests that crosstalk will have a more deteriorating effect on the accuracy of impedance-based temperature estimation when using higher measurement frequencies. Nevertheless, even when using lower measurement frequencies, crosstalk may still cause the impedance-based temperature estimates to be inaccurate. The same phenomenon is observed for $Z_1^\star(f)$. Note that, for the measurements in Figure 4, the cells were not electrically connected to each other, although the crosstalk would be the same if they were. The presence of crosstalk interference means that the off-diagonal terms in $Z(f)$ in (6) (ie, the crosstalk impedances) are nonzero and hence need to be considered in EIS measurements, which can be

done by using a model of the crosstalk behaviour as developed by Raijmakers et al.[20]

3.2 | SoC and *T* dependency of crosstalk

To effectively compensate for crosstalk in an impedance-based temperature estimation method, it is also necessary to investigate the dependence of crosstalk on temperature *T* and SoC of the batteries, which has not been done by Raijmakers et al.[20] Therefore, new impedance measurements have been performed with the two-cell setup as depicted in Figure 2A, which is the same setup that has been used by Raijmakers et al.[20] In particular, the elements of the frequency-response matrix $Z(f, T, \text{SoC})$ from (6) with $N = 2$ have been approximated by performing $L = 64$ impedance measurements at every grid point in *f*, *T*, and SoC so as to mitigate the effect of the measurement noise v (more details of the impedance model will be introduced in Section 5).

The results are shown in Figure 5 by means of Bode plots of the individual cell impedance Z_{11} and the crosstalk impedance Z_{12} (note that the scaling of the axis in Figure 5A,B is equal, as well as the scaling of Figure 5C,D. It should be noted that the impedance Z_{22} is

similar to Z_{11} and Z_{21} is similar to Z_{12}. Figure 5A,B shows the dependence on *T* for Z_{11} and Z_{12}, whereas Figure 5C, D shows the dependence on SoC. In Figure 5A, it can be seen, as expected from performing impedance-based temperature estimation, that the individual cell impedance Z_{11} depends on temperature *T*. This can also be observed from Figure 3, where the measured Z_{11} is shown in a Nyquist plot. The crosstalk impedance Z_{12} is, however, independent of temperature. Regarding the dependency on SoC, Figure 5C shows that the individual cell impedance slightly depends on SoC.[7] Similar to being independent of temperature, the crosstalk impedance in Figure 5D is also independent of SoC. This allows the matrix *Z* in (6) to be simplified by using the fact that the off-diagonal (crosstalk) terms depend neither on SoC nor on temperature *T*. This also simplifies temperature estimation in the presence of crosstalk.

4 | (DIS)CHARGE CURRENTS

In this section, we will discuss the inclusion of (dis) charge currents $D(f)$ in the temperature estimation method, as was indicated in (6). Incorporation of $D(f)$ in
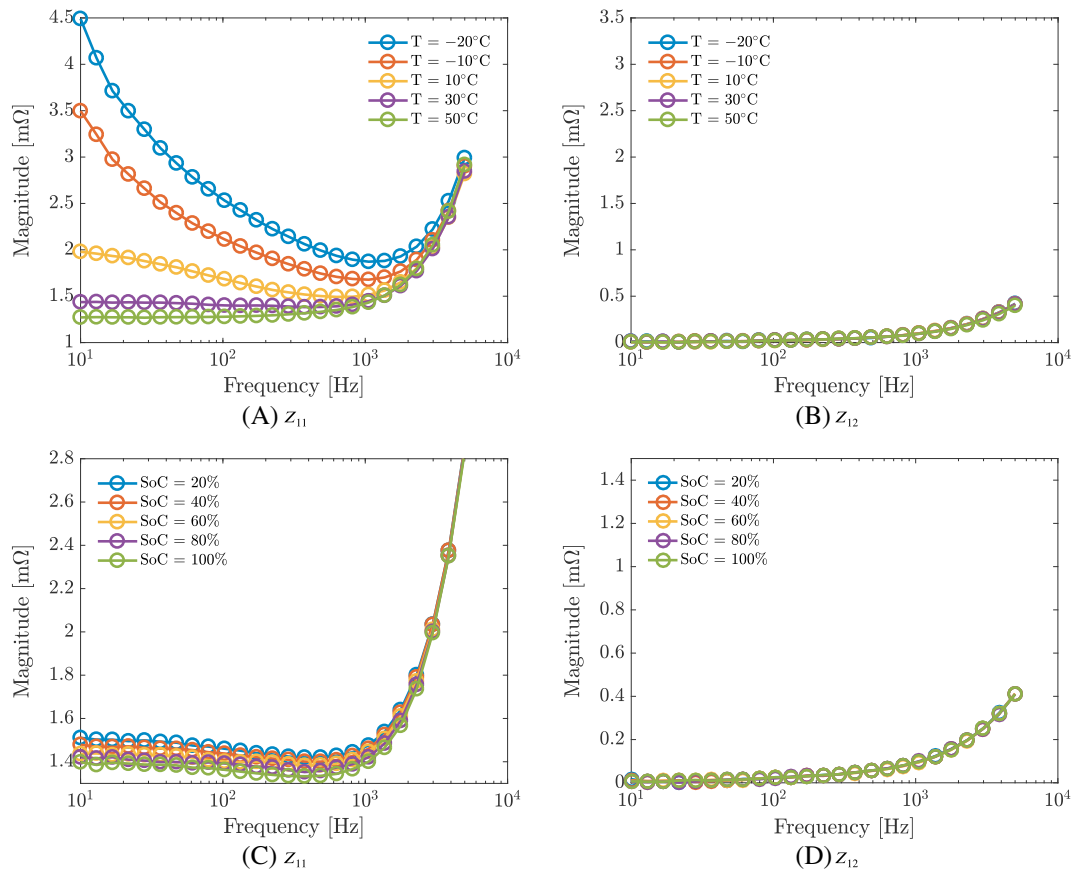

FIGURE 5 Influence of temperature *T* and state-of-charge (SoC) on $Z(f)$ at SoC = 60% and $T = 30°$C for the top and bottom plots, respectively [Colour figure can be viewed at wileyonlinelibrary.com]

the temperature estimation is relevant, because in real battery applications, impedance-based temperature estimation needs to be performed while the battery is used, ie, when $D(f) \neq 0$. The (dis)charge current $D(f)$ is flowing through each cell in addition to the current $I_i(f)$ drawn by the EIS measurement and will affect the measured voltages $V_i(f)$, as can be seen from (6). This will act as a disturbance in the EIS measurements and will result in inaccurate EIS measurements. As mentioned in the introduction of this paper, it is not possible to synchronise the impedance measurements with the measurement of the (dis)charge current (because of limitations of the measurement device). Consequently, the effect of the (dis)charge current on the impedance measurement *cannot be compensated for* in this particular case. Still, inclusion of the (dis)charge current in the framework for temperature estimation is useful since it can also be used to *analyse* the effect of the (dis)charge current on the temperature estimation. Therefore, in this paper, the inclusion of (dis)charge current will be used as a tool for analysis so as to arrive at an optimal temperature estimation method, despite the (uncompensated) presence of the disturbance caused by the (dis)charge current. However, for future use (in case of synchronisation of the measurements), the inclusion of the (dis)charge current in the estimation framework may be used to compensate for the effect of this (dis)charge current on the estimation accuracy.

It should be noted that the (dis)charge current can interfere with the EIS measurement from two perspectives. From a signal-integrity perspective, the (dis)charge current and the corresponding frequency content of this signal can interfere with the measured battery voltage, which is a *measurement* artefact. From an electrochemical perspective, on the other hand, (relatively large) (dis)charge currents will drive the battery out of the electrochemical equilibrium, causing the impedance to change, which can be seen as a *model* artefact.[30,31] In this paper, we consider the *measurement* artefacts on the EIS measurement introduced by the (dis)charge current. Incorporating the *model* artefacts in the analysis can be seen as an extension and a valuable next step to this work. The relation between the impedance and the relaxation period after (dis)charge has been shown in previous studies.[30,31] Subsequently, Zhu et al[32] have used this relation to correct the measured impedance under operating conditions for this electrochemical effect in order to perform impedance-based temperature estimation.

In this section, we will develop two methods to incorporate an estimate of $D(f)$, denoted by $\hat{D}(f)$, in the temperature estimation method of Section 2.1. In particular, we will consider the (deterministic) case where the (dis)charge current can be measured synchronously with the impedance measurements and, therefore, can be used to compensate the measured $Z(f)$ for the effect of $D(f)$. This allows for constructing a deterministic model of $D(f)$ using the measured (dis)charge current. We will also consider the case that reflects the experimental setup of this paper. Namely, the (dis)charge current cannot be measured synchronously with the impedance measurements and, therefore, the measured current is not suitable for directly compensating $Z(f)$. In this case, we model $D(f)$ stochastically as a random signal, which allows us to analyse the (deteriorating) effect of $D(f)$ on the temperature estimation.

4.1 | Deterministic modelling

Let $d(t)$ denote the (dis)charge current during a time window $t \in [\hat{t}, \hat{t}+\tau]$ in which the EIS measurement takes place, where τ denotes the measurement time. An example of a typical (dis)charge current can be found in Figure 6A, where an actual measured (dis)charge current from a drive test is shown, which has been generated by an acceleration-deceleration cycle with an electric vehicle over a period of 120 seconds with a sampling frequency of $f_s = 100$ kHz. In this figure, the negative current can be seen as current driving the vehicle and the positive current as current flowing into the battery during regenerative braking. Because of the relatively short periods of charge and discharge in Figure 6A, in combination with the fact that the (dis)charge current is approximately zero-mean over this period, the SoC of the battery pack will be (approximately) constant for this cycle. It is important to note that this relatively short driving cycle has been selected in order to obtain the properties of the (dis)charge current of an EV since the goal of our study is to extend the method of impedance-based temperature estimation towards its application in battery packs. Namely, it has already been shown in previous studies that impedance-based temperature estimation can be applied to more general driving cycles with relatively large changes in SoC.[9,26]

The current signal $D(f)$ is given by the Fourier transform of the signal $d(t)$. As an estimate of this signal $D(f)$, we can take

$$\hat{D}(f) = \int_{\hat{t}}^{\hat{t}+\tau} d(t)e^{-2\pi jft}\mathrm{d}t, \qquad (10)$$

meaning that $D(f) \approx \hat{D}(f)$ can be used in the temperature estimation method and accounts for the effect of (dis)charge current in the temperature estimation. Note that (10) can be approximated as a fast Fourier transform. This, however, requires that $d(t)$ can be measured in real

time and synchronously with the EIS measurements. This might be difficult to realise in practice and currently, the setup with the SCS of Figure 2 is limited to measuring the impedance and (dis)charge current separately (ie, not synchronously). Therefore, we will also consider a stochastic approach that can be used to analyse the effect of the (dis)charge current on the temperature estimation.

4.2 | Stochastic modelling

In case the (dis)charge current $d(t)$ cannot be measured in real time, or not synchronously with the EIS measurements, we can model the (dis)charge current as a random variable in the frequency domain for the purpose of analysing the effect of this current on the temperature estimation. To be more precise, we model $D(f)$ as a zero-mean Gaussian random variable with frequency-dependent variance $\sigma^2(f)$.[3] The stochastic model $\hat{D}(f)$ cannot be used to compensate for $D(f)$, since the model does not capture $D(f)$ in a certain time window $t \in [\hat{t}, \hat{t} + \tau]$ synchronously with the EIS measurements. However, by modelling the signal as a random variable in the frequency domain, it is possible to analyse the effect of (dis)charge current on temperature estimation and to quantify the average error on the temperature estimation caused by the pack current. Namely, it can be stated that the variance $\sigma^2(f)$ of this random variable is equal to the power spectral density (PSD) of the random signal $d(t)$ and can be interpreted as the representation of $d(t)$ in the frequency domain; see Childers and Miller.[33,chapter10] The PSD can be computed efficiently using, eg, Matlab using a realisation of $d(t)$ under the assumption that $d(t)$ is a stationary random variable. For the (dis)charge current given in Figure 6A, the corresponding PSD is given in Figure 6B,

in which we indicate the upper-peak envelope of the PSD in red to prevent the analysis to prefer local minima in the spectrum. This envelope will be used to characterise $D(f)$ and thus the variance $\sigma^2(f)$ per frequency. This will be used to analyse the effect of the (dis)charge current on the temperature estimation in this paper.

5 | TEMPERATURE ESTIMATION IN PRESENCE OF CROSSTALK AND (DIS)CHARGE CURRENTS

Using the results of modelling crosstalk and (dis)charge current disturbances from the previous two sections, the temperature estimation method given by (4) in Section 2.1 is extended as follows. The perceived battery impedance $Z_m^\star$ of cell m in an N-cell battery pack in the presence of crosstalk and (dis)charge currents is now of the form

$$
\begin{aligned}
Z_m^\star(f, T, \text{SoC}) &= \frac{V_m(f, T, \text{SoC})}{I_m(f, T, \text{SoC})} \\
&= \sum_{n=1}^{N} \left(Z_{mn}(f, T, \text{SoC}) \frac{I_n(f) + D(f)}{I_m(f)} \right),
\end{aligned}
\tag{11}
$$

which follows from (6). In (11), the (dis)charge current term $D(f)$ depends on the instantaneous (dis)charge current and is a random variable in this study. Note that it is also possible to take a deterministic approach as shown in Section 4.1, if the measurement of the (dis)charge current can be synchronised with the impedance measurements. The crosstalk phenomenon, however, is deterministic and, hence, the model can be extended to include the crosstalk terms, which allows the estimator to compensate for crosstalk interference. Now, the impedance model $\hat{Z}_m$:
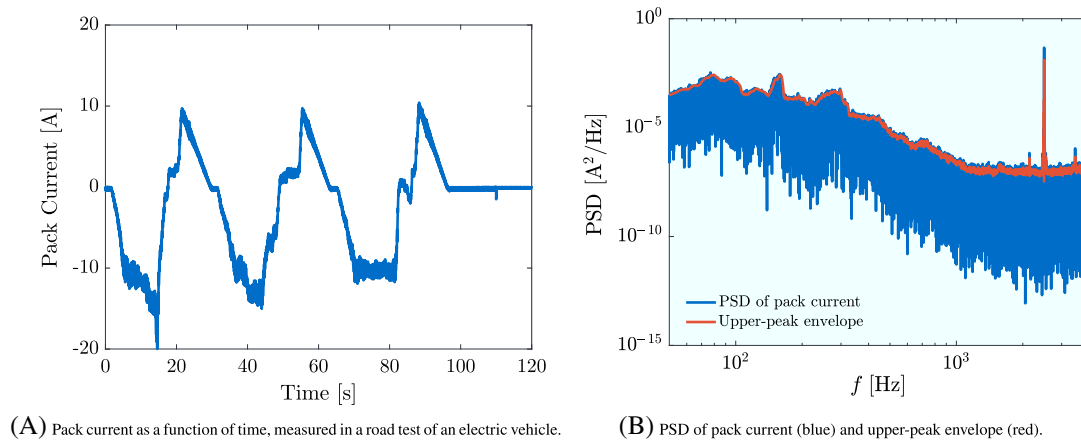

(A) Pack current as a function of time, measured in a road test of an electric vehicle.

(B) PSD of pack current (blue) and upper-peak envelope (red).

FIGURE 6 Pack-current measurement of an electric vehicle. (A) Pack current as a function of time, measured in a road test of an electric vehicle. (B) Power spectral density (PSD) of pack current (blue) and upper-peak envelope (red) [Colour figure can be viewed at wileyonlinelibrary.com]

$\mathbb{R}^3 \to \mathbb{C}$ of the perceived cell impedance $Z_m^\star$ of cell m is given by

$$\hat{Z}_m(f_r, T_r, \text{SoC}_r) = \sum_{n=1}^{N} \hat{Z}_{mn}(f_r, T_r, \text{SoC}_r) \frac{I_n(f_r)}{I_m(f_r)} \quad (12a)$$

by averaging several measured impedances as

$$\hat{Z}_{mm}(f_r, T_r, \text{SoC}_r) = \frac{1}{L} \sum_{i=1}^{L} Z_{mm}(f_r, T_r, \text{SoC}_r) + v_i, \quad (12b)$$

$$\hat{Z}_{mn}(f_r) = \frac{1}{L} \sum_{i=1}^{L} Z_{mn}(f_r) \frac{I_m(f_r)}{I_n(f_r)} + v_i \quad n \neq m, \quad (12c)$$

where $L \in \mathbb{N}$ is the number of measurements taken for each combination of grid points f_r, T_r, and SoC_r, and, as mentioned previously, no compensation for $D(f)$ will be applied and, therefore, it is not considered when constructing $\hat{Z}_m$ in (12a). We can model the battery impedance (ie, the diagonal entries in Z in (6)) by taking $D(f) = 0$ and $I_n(f) = 0$ for all $n \neq m$ and subsequently measure the crosstalk interference (ie, the off-diagonal entries in Z in (6)), while still taking $D(f) = 0$, ie, not (dis)charging the battery. Although the cells in the pack are matched, the measured impedance of the battery cells can vary, eg, because of slight differences in the mounting or wiring of the measurement equipment. Therefore, an impedance model of every cell m should be constructed, in order to prevent modelling errors from affecting the temperature estimation. Note that, based on the results in Section 3, we use that Z_{mn} only depends on frequency for $n \neq m$. Recall that the model $\hat{Z}_m(f_r, T_r, \text{SoC}_r)$ is defined as a lookup table at the selected grid points. Using interpolation to obtain values in between grid points, the model in (12) can be considered as $\hat{Z}_m(f, T, \text{SoC})$ (ie, a lookup-table model with built-in interpolation function).

The modelled impedance $\hat{Z}_m$ from (12) and the measured battery impedance, which is of the form of (11) with additive measurement noise, ie, $Z_m^{\text{meas}} = Z_m(f, T, \text{SoC}) + v$, are now substituted into the nonlinear least-squares estimator of (4) to estimate the temperature of each cell in the pack. It should be noted that the model in

TABLE 1 Measurement settings for constructing $\hat{Z}$

Temperature T	$-20°C, -10°C, 0°C, +10°C, +20°C, +30°C, +40°C, +50°C$
Frequency f	25 log-spaced f: $10\,\text{Hz} \leq f \leq 5\,\text{kHz}$
SoC values	20%, 40%, 60%, 80%

Abbreviation: SoC, state-of-charge.

(12) illustrates the fundamental difference between impedance-based temperature estimation at a single-cell level or in a battery pack. Namely, for temperature estimation in a single-cell application, one can construct a lookup table that directly reads the impedance model $\hat{Z}_m$ as constructed with (3), whereas temperature estimation for a battery pack involves constructing $\hat{Z}_m$ using (12) with a lookup table that reads all elements Z_{mn} of the frequency-response matrix given in (6). Also note that, although we based the model in (12) on $D(f) = 0$, $D(f)$ will be included in the accuracy analysis as a zero-mean random Gaussian variable in Z_m^{meas} in order to evaluate the performance of the estimator in presence of (dis)charge currents.

6 | ACCURACY ANALYSIS

In this section, Monte Carlo simulations are performed in order to analyse the accuracy of the extended method for temperature estimation in terms of the MSE, for different settings of f and α. The analysis is performed for a range of possible battery temperatures and SoC values under different conditions, such as the presence of crosstalk and (dis)charge-current disturbances. The analysis can then be used to arrive at a set of values for f and α, which yield the most accurate temperature estimate $\hat{T}$.

6.1 | Setup of the analysis

The experiments are conducted on the setup in Figure 2A, which consists of $N = 2$ cells and corresponds to the frequency-response matrix from (6), given by

$$Z(f, T, \text{SoC}) = \begin{bmatrix} Z_{11}(f, T, \text{SoC}) & Z_{12}(f) \\ Z_{21}(f) & Z_{22}(f, T, \text{SoC}) \end{bmatrix}. \quad (13)$$

The impedance models $\hat{Z}_{mm}$ and $\hat{Z}_{mn}$ of the elements Z_{mm} and Z_{mn} of (13) can be obtained through (12) for

TABLE 2 Settings for $\hat{Z}_m$ and Z_m^{meas} in Monte Carlo simulations at SoC = 60%

	Case A	Case B	Case C	Case D
$\hat{Z}_m$	$I_m \neq 0$	$I_m \neq 0$	$I_m \neq 0$	$I_m \neq 0$
	$I_n = 0$	$I_n = 0$	$I_n = 0$	$I_n \neq 0$
Z_m^{meas}	$I_m \neq 0$	$I_m \neq 0$	$I_m \neq 0$	$I_m \neq 0$
	$I_n = 0$	$I_n \neq 0$	$I_n = 0$	$I_n \neq 0$
	$D(f) = 0$	$D(f) = 0$	$D(f) \neq 0$	$D(f) \neq 0$

Abbreviation: SoC, state-of-charge.

$N = 2$, using the measurement settings in Table 1 for f, T and SoC. For the purpose of this modelling procedure, the number of measurements for a certain operating point in f, T and SoC is taken to be $L = 64$. The number of EIS measurements L that can be taken at each temperature is limited by the rate of discharge of the battery that occurs during the impedance measurements (as the measurement current of the impedance measurements has a nonzero DC component). Therefore, $L = 64$ is assumed to be sufficiently large to average out measurement noise v, yet small enough to not affect the SoC of the batteries significantly. For the accuracy analysis, the approach is the same as for the Monte Carlo analysis in our previous work.[7] Recall that, for the analysis and validation, the two-cell battery pack is used since the aim of this study is to develop a solid proof of concept for developing the method of impedance-based temperature estimation towards its application in battery packs. The extension to larger battery packs can be seen as an important next step in the development of the method.

The accuracy analysis consists of four cases, where

A. Neither crosstalk nor (dis)charge currents are present in the temperature estimation.
B. Crosstalk is present but not accommodated for in the temperature estimation.
C. (Dis)Charge currents are present, but not accommodated for, and crosstalk is not present.
D. Both crosstalk and (dis)charge currents are present, and crosstalk is accommodated for in the temperature estimation.

Recall that the case where both crosstalk and (dis)charge current are present and both accommodated for in the temperature estimation is not considered, since the (dis)charge current cannot be measured synchronously with the battery impedance using the SCS. For each case, different combinations of measurement conditions (ie, Z_m^{meas}) and models (ie, $\hat{Z}_m$) are considered, which are defined by the settings in Table 2. The model $\hat{Z}_m$ for each case is now constructed using the settings in Table 2 and the modelled elements of Z in (13), ie, the impedance models $\hat{Z}_{mm}$ and $\hat{Z}_{mn}$ in (12b) and (12c), respectively. For example, in case A, where we simulate impedance-based temperature estimation without crosstalk interference or (dis)charge currents (ie, as presented in our previous study[7]), Table 2 reads that the modelled impedances for $N = 2$ cells, ie, $\hat{Z}_m$ with $m = \{1, 2\}$, are constructed with $I_2(f) = 0$ for $\hat{Z}_1$ and $I_1(f) = 0$ for $\hat{Z}_2$. In other words, $\hat{Z}_1$ and $\hat{Z}_2$ are the single-cell impedance models as used in our previous study[7] (which is also true for cases B and C). For each case, this results in a model $\hat{Z}_m$, which comprises a three-dimensional lookup table

of the impedance of each cell with a temperature-frequency-SoC grid. A finer temperature-frequency-SoC grid is further obtained by cubic spline interpolation. Similarly, the measured impedances Z_m^{meas} are obtained with the settings from Table 2. As mentioned previously, the influence of (dis)charge current $D(f)$ can also be evaluated by modelling $D(f)$ in a stochastic manner; see Section 4.2. For cases A and B, however, $D(f)$ is not considered, and therefore, $D(f) = 0$ in Table 2.

On the basis of the model $\hat{Z}$ of the impedance Z in (13), and using the estimator in (4), Monte Carlo simulations (see, eg, Rubinstein and Kroese[34]) have been performed to evaluate the estimation accuracy using measurement noise v with a SD σ that depends on frequency and is obtained from measurement data; see Figure 2B. For the simulations, SoC = 60% is chosen and thus used as a set-point in the impedance model $\hat{Z}_m$ in (12). However, even if a different SoC is chosen, the analysis method would remain the same. The input distribution of measured impedance values for the Monte Carlo simulations (ie, Z_m^{meas} for evaluation in (4)) is generated by taking the sum of the modelled impedance $\hat{Z}_m$ and a distribution of the measurement noise v. Similar to the methodology used in our previous work,[7] the number of Monte Carlo simulations is selected as $N_{\text{MC}} = 10^4$. This ensures a confidence bound of greater than or equal to 95% of all estimates being within $\pm 0.2°C$.[29] For more details on the Monte Carlo simulations, see Beelen et al.[7] Note that the analysis in this section is performed for only one of the cells in the two-cell battery pack. Because of symmetry, the results of the estimation method would be similar (yet not the same because of small differences in the battery impedance) for the other cell and is therefore not repeated in the following analysis. Also, recall that the influence of crosstalk and (dis)charge current on the temperature estimation is analysed using the models of these disturbances as presented in Sections 3 and 4, respectively. For the experimental validation with the two-cell battery pack in Section 7, the synthesised estimation method (with the f and α found in this analysis) will be subject to actual crosstalk and (dis)charge current. Finally, a temperature range from $-10°C$ to $40°C$ will be used for both the analysis in this section as well as the validation in Section 7. This range has been chosen so as to ensure a safe test environment for providing a proof of concept for the proposed method of impedance-based temperature estimation in battery packs. Moreover, this temperature range is a reasonable assumption for the battery temperatures encountered during (normal) operation of the battery cell and has been used in a number of other studies as well.[7,12,16] Nevertheless, for future research and validation, the temperature range can be extended as the principle of impedance-based temperature
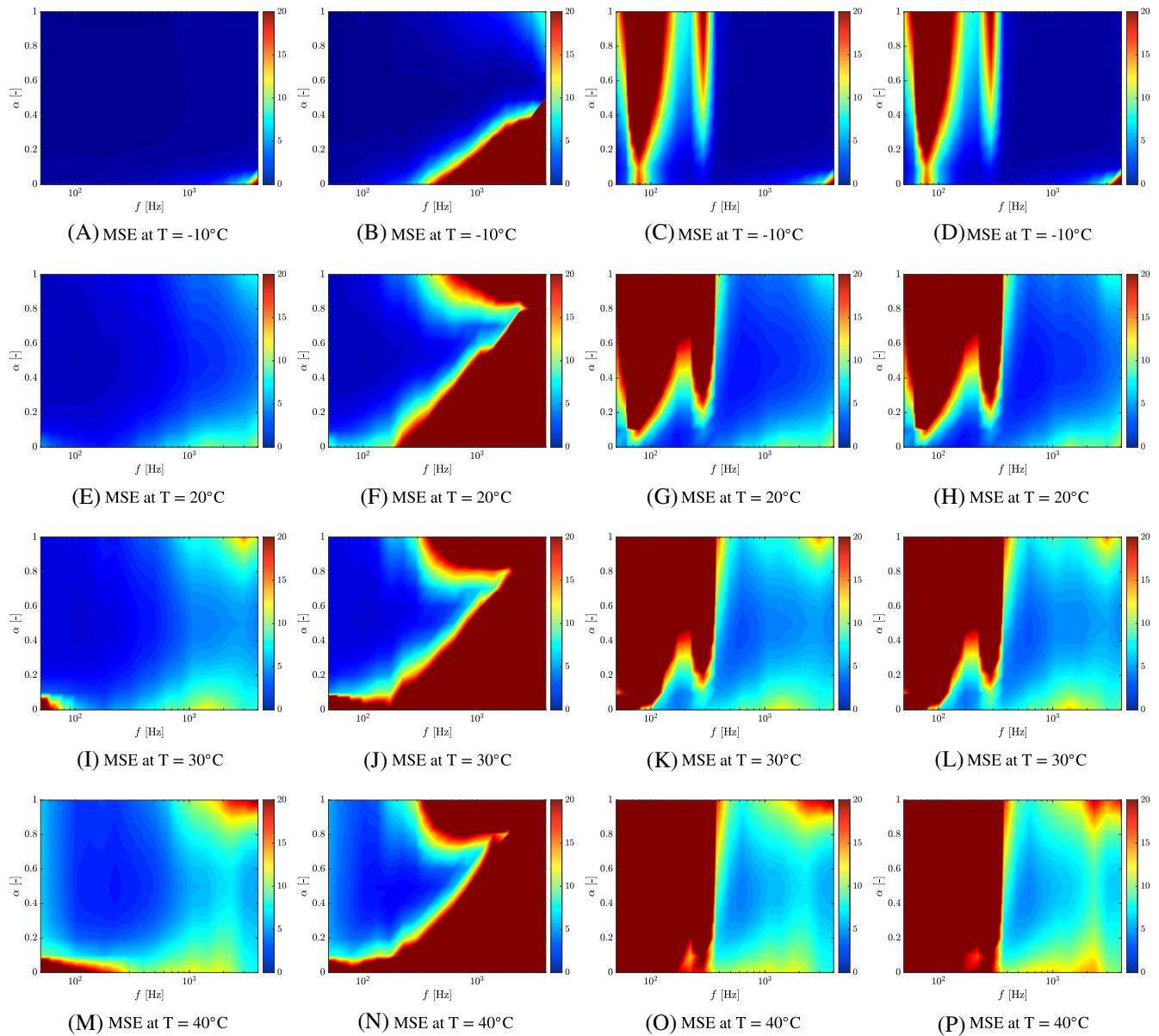
FIGURE 7 Mean-square estimation error (MSE) at different temperatures (in ascending order from top to bottom) and SoC = 60% as a function of f and α for case A (first column), case B (second column), case C (third column), and case D (fourth column). The colour in each plot corresponds to the colour bar representing MSE expressed in $°C^2$. SoC, state-of-charge [Colour figure can be viewed at wileyonlinelibrary.com]

estimation has been shown to be valid for a wider range of temperatures.[8,9,15]

6.2 | Temperature estimation without crosstalk

In the case of temperature estimation in the absence of crosstalk and (dis)charge currents, the simulation settings used for generating the models and the measurements are described in Table 2, case A. The resulting MSEs over a range of f, α, and T are shown in the first column of

plots in Figure 7 and are in agreement with the results found in our previous study,[7] although the analysis in this case is performed on a different cell type. It can be seen that the MSE increases towards higher frequencies. Moreover, this effect becomes more pronounced at higher temperatures. This indicates that the sensitivity of the battery impedance with respect to temperature decreases towards higher temperatures and higher frequencies. This effect has also been observed in our previous study[7] and corresponds to the fact that low frequencies for impedance-based temperature estimation are preferable.[11,12,15] In terms of settings for f and α, the results of case A indicate

that there is a relatively large range of values for f and α that yield similar performance in terms of the MSE of temperature estimation.

6.3 | Temperature estimation with crosstalk

For case B, the analysis from the previous case, where no crosstalk was present, is repeated with the same impedance models $\hat{Z}_1$ and $\hat{Z}_2$. However, the measured impedances Z_1^{meas} and Z_2^{meas} are now obtained with both $I_1(f) \neq 0$, $I_2(f) \neq 0$, and $D(f) = 0$ as denoted in Table 2, case B. In other words, the impedance measurements are disturbed by crosstalk. However, since $\hat{Z}_1$ and $\hat{Z}_2$ are the same as for case A, this interference is not taken into account in the temperature estimation. In other words, no compensation for the crosstalk interference is applied. The resulting MSE plots are shown in the second column of plots in Figure 7. As expected, the MSE increases with higher frequencies since the crosstalk becomes more dominant at higher frequencies as shown by Raijmakers et al.[20] For the selection of f and α, these results imply that we are forced to choose a lower f such that the crosstalk interference (if not compensated for) has limited (or no) effect on the temperature estimation.

6.4 | Temperature estimation with (dis)charge currents

Up to this point, we have seen that low frequencies are preferably used for temperature estimation. In practice, however, dynamic (dis)charge currents will be present in, eg, automotive applications. We will now investigate how this phenomenon will affect the temperature estimation. The first case (ie, case A without crosstalk) is now repeated, but the (dis)charge current $D(f) \neq 0$ and $D(f)$ is used in Z_m^{meas} as stochastically defined in Section 4.2 (ie, a disturbing (dis)charge current is added to the simulation). Note that the phase shift between the measured voltage and the (dis)charge current varies; therefore, no phase information can be extracted from the frequency spectrum of the (dis)charge current. Hence, for $D(f)$, the phase is obtained from a set of normally distributed pseudo-random numbers. The resulting MSE plots are shown in the third column of plots in Figure 7. It can be observed that the MSE is larger for lower frequencies, since also the amplitude of the (dis)charge current is larger at lower frequencies as shown in Figure 6B (ie, the (dis)charge current affects the temperature estimation). It can also be observed that the MSE is larger for α closer to 1. This indicates that the (dis)charge currents have a larger influence on the real part of the impedance, which has also been found by Koch and Jossen.[16] In conclusion, this analysis indicates that, in case of (dis)charge currents, higher frequencies should be chosen to obtain the most accurate temperature estimate.

6.5 | Compensating for crosstalk

In this case, the Monte Carlo simulations are performed by including both crosstalk interference and (dis)charge currents. This means that Z_1^{meas} and Z_2^{meas} are measured with both $I_2(f) \neq 0$, $I_1(f) \neq 0$, respectively, and $D(f) \neq 0$ as denoted in Table 2. This means that both crosstalk and (dis)charge currents interfere with the impedance measurements and thus affect the impedance-based temperature estimation. Since crosstalk mainly affects the high-frequency region (see case B) and (dis)charge currents affect the low-frequency region (see case C), this suggests that it may not be possible to find suitable settings for f and α if the frequency ranges in which these disturbances affect the temperature estimation overlap. Unfortunately, these frequency ranges do indeed (slightly) overlap as can be seen from (visually) comparing the dark red areas of cases B and C in Figure 7 (see Section 6.6 for more details). Fortunately, it is possible to compensate for the effect of the crosstalk interference by using the crosstalk model as introduced in Section 3. Therefore, in contradiction to the previous cases, crosstalk models are also included when constructing $\hat{Z}_1$ and $\hat{Z}_2$ in (12), ie, the terms $\hat{Z}_{mn}$ in (12) are no longer zero. The resulting MSE plots are shown in the fourth column of plots in Figure 7. Since the crosstalk is captured by the models, the MSE plots are similar to the case where crosstalk is absent, but with the added disturbance of (dis)charge currents (ie, case C), which causes the MSE to be larger at low frequencies.

6.6 | Selection of f and α

The plots in Figure 7 can be used to find the parameters f and α that yield the smallest MSE for temperature estimation in certain conditions. The plots show that, generally, for all four cases, the MSE is larger at high temperatures compared with that in lower temperatures. This is in agreement with the fact that the sensitivity of the battery impedance decreases towards higher temperatures. Therefore, we can use the MSE at $T = 40°C$ (ie, Figure 7M-P) for selecting f and α for each case, since it gives the worst-case MSE. For example, consider the case where there is no crosstalk and where no (dis)charge currents are injected in Figure 7M. The smallest MSE is found around $f = [100, 300]$ Hz and $\alpha = .5$, which is also

TABLE 3 Optimal values of f and α from analysis, including resulting average MSE in simulation (Section 6) and validation (Section 7)

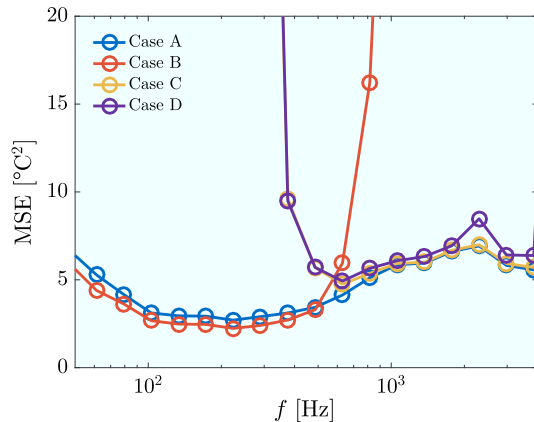| Analysis Case	f, Hz	α	avg. MSE, $^\circ C^2$	
			sim.	val.
Case A. Without crosstalk	133	0.5	1.1	1.1
Case B. With crosstalk	133	0.5	1.1	1.1
Case C. With (dis)charge currents	630	0.5	2.3	4.0
Case D. With crosstalk compensated	630	0.5	2.3	3.8

Abbreviation: MSE, mean-square estimation error.

FIGURE 8 Mean-square estimation error (MSE) obtained from simulation study as a function of frequency for each of the four cases at $T = 40^\circ C$ and SoC = 60%, with $\alpha = .5$. SoC, state-of-charge [Colour figure can be viewed at wileyonlinelibrary.com]

a favourable setting for lower temperatures, ie, Figure 7A, E, I. The results for a similar analysis for the other cases can be found in Table 3, which shows that $\alpha = .5$ provides the best results in all four cases. Alternatively, for all four cases, the MSE can be depicted as a function of frequency f, while taking $\alpha = .5$. This is depicted in Figure 8 and also allows the selection of a frequency f that results in the smallest MSE for each case.

Moreover, Figure 8 gives an interesting insight in how the choice of measurement frequency f is affected by the type of measurement case that is considered. Namely, in the absence of (dis)charge currents (ie, cases A and B), selecting a relatively low f in the range of $f = [100, 300]$ Hz results in the smallest MSE, where it should be noted that for very low f, the MSE increases again because of the measurement noise of the SCS as depicted in Figure 2B. However, in the presence of (dis)charge currents (ie, cases C and D), the preferred f is pushed towards higher frequencies, because of the fact that the amplitude of the PSD in Figure 6B is larger for lower frequencies. More precisely, since there is no compensation for the (dis)charge current in this work and the disturbance caused by the (dis)charge current is more pronounced for relatively low frequencies, a higher frequency should be chosen so as to

achieve a smaller MSE for the temperature estimation. Note that there is no difference between cases C and D in this reasoning since in case C, crosstalk is not present, while in case D, crosstalk is present but compensated for in the temperature estimation. Also, the preferred f is influenced by the low sensitivity of the battery impedance with respect to temperature at higher frequencies and by crosstalk, if it is not compensated for as shown in case B.

It is important to note that crosstalk compensation is indeed necessary in this particular case (ie, with this type of battery cell, this particular experimental setup, and the selected (dis)charge current profile). Namely, since low measurement frequencies are affected by the (dis)charge currents and high measurement frequencies are affected by crosstalk interference, one might argue that there could be a (mid-range) frequency band in between both disturbances that is not affected and thus suitable for impedance-based temperature estimation without crosstalk compensation. However, comparing cases B and C in Figure 8 gives the following interesting insight. Following the line for case C (which is difficult to see as it is underneath the purple line of case D for lower frequencies), starting at approximately 400 Hz, it can be seen that from a certain frequency onwards (approximately 600 Hz), the (dis)charge current does not affect the MSE compared with the base case with no disturbances, ie, case A. However, at that same frequency, the crosstalk (ie, the red line) starts to have an effect on the MSE (and this effect becomes stronger for higher frequencies). In other words, in this case, crosstalk compensation is indeed necessary to arrive at the optimal MSE in the presence of both disturbances.

In conclusion, when both crosstalk and (dis)charge-current interference are present, a trade-off is found in selecting f as depicted in Figure 8, case D (purple line). Therefore, Table 3 shows the optimal design parameters. For cases A and B, the frequency $f = 133$ Hz (from the range $f = [100, 300]$ Hz) is chosen, and for cases C and D, $f = 630$ Hz is selected. Note that this analysis and the conclusions drawn here are specific to this particular cell, the pack arrangement, and measurement device used in this paper. Nevertheless, the analysis framework used in this paper is general and can be applied to other types of
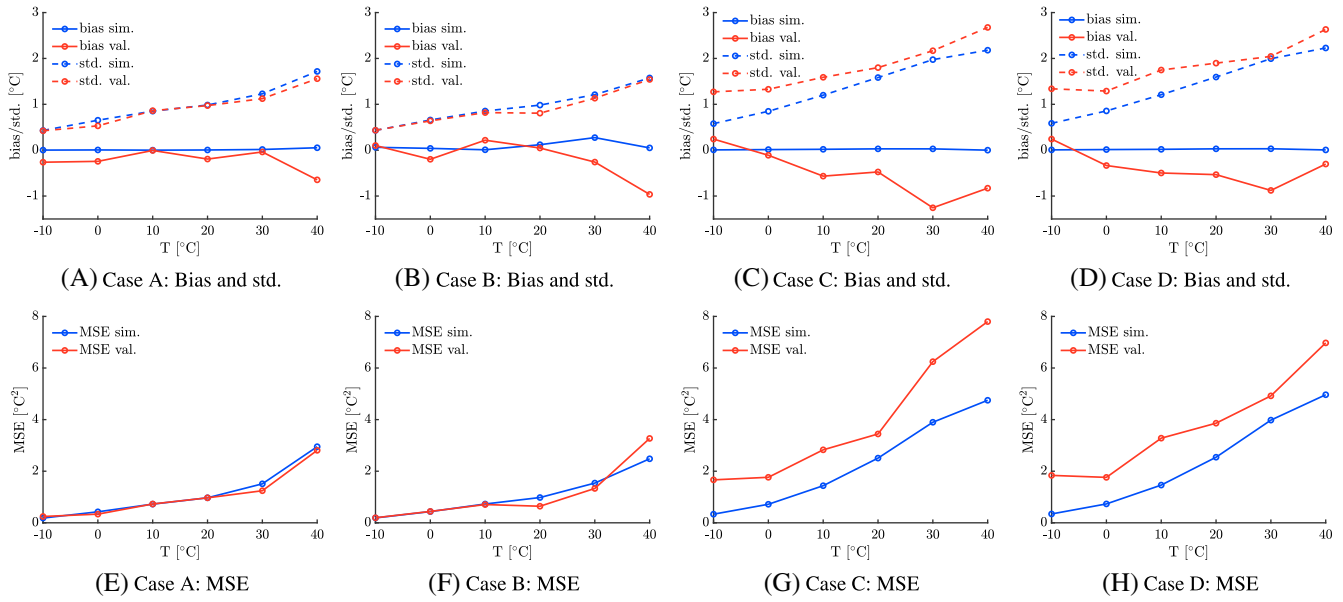
FIGURE 9   Bias, SD (std.), and mean-square estimation error (MSE) as a function of the actual battery temperature T for cases A to D as denoted in Table 3. Blue lines and red lines depict simulation results and validation results, respectively. (A) Case A: bias and std. (B) Case B: bias and std. (C) Case C: bias and std. (D) Case D: bias and std. (E) Case A: MSE. (F) Case B: MSE. (G) Case C: MSE. (H) Case D: MSE [Colour figure can be viewed at wileyonlinelibrary.com]

cells, other arrangements of battery packs, and other measurement devices as well.

7 | EXPERIMENTAL VALIDATION

Using the optimal design choices for f and α in Table 3, the temperature estimation method will be validated experimentally in this section. This validation has been performed on the two-cell battery pack of Figure 2A for all four cases discussed in Section 6. Similar to the accuracy analysis in Section 6, the temperature estimation involves solving (4) for a set of validation measurements, using the appropriate model for each particular case, identical to the cases and models discussed in Section 6 and denoted in Table 2. A number of $N_{val} = 64$ validation measurements have been taken for each case and at each temperature $T \in \{-10, 0, 10, 20, 30, 40\}°C$, where again the cells have been maintained at SoC = 60%. Although N_{val} is substantially smaller than the number of Monte Carlo simulations $N_{MC} = 10^4$ used in Section 6, it is sufficient for the experimental validation. Note that the batteries have been at rest at a particular temperature for a period of 3 hours before the experiment, meaning that the batteries were in thermal equilibrium when the impedance measurements were performed.

It is important to note that the experimental validation focuses solely on the method presented in this paper,

and no comparison with other methods is included. To the best of the knowledge of the authors, there have not yet been any studies that have investigated the applicability of impedance-based temperature estimation to battery packs since the existing literature focuses predominantly on impedance-based temperature estimation for single battery cells, typically under laboratory conditions. Therefore, a comparison is simply not possible. For a comparison of the existing techniques for impedance-based temperature estimation at the single-cell level, the reader is referred to Beelen et al.[7]

In Figure 9, the (sample estimates of the) bias, SD, and MSE of the estimated temperature $\hat{T}$ are depicted for each case. For comparison, the simulation results (obtained by the Monte Carlo simulations) of the analysis in Section 6 are also depicted for the selected f and α. The (average) MSE, resulting from the combination of bias and SD as shown in (8), is denoted in Table 3.

7.1 | Temperature estimation without crosstalk

The measurements for the case where no crosstalk is present, together with the models $\hat{Z}_1$ and $\hat{Z}_2$, as mentioned in Section 6, and the selected α have been substituted into (4). The results for bias and SD of the estimation are shown in Figure 9A. The corresponding MSE as defined in (8) is depicted in Figure 9E. The average of the MSE

over all temperatures can be found in Table 3. Overall, both bias and SD are in agreement with the results from the analysis in Section 6 and subsequently, also the MSE of the validation is in agreement with the simulation. These validation results indicate that, in this case, the temperature can be estimated with an accuracy of $\pm1°C$ as shown in Figure 9A. The difference between simulations and measurements for both bias and SD may be caused by modelling inaccuracies or a mismatch in SoC in either the modelling procedure or the validation measurements or both.

7.2 | Temperature estimation with crosstalk

The results for the case where crosstalk is present, but not compensated for in the estimation, can be found in Figure 9B,F and Table 3. Since the selected frequency f is low, the influence of crosstalk on T estimation is not dominant. The results are found to be in agreement with the analysis and similar to case A, the temperature can be estimated with an accuracy of $\pm1°C$ as shown in Figure 9B. Note that differences between simulation and measurement may be due to similar influences as mentioned with case A.

7.3 | Temperature estimation with (dis)charge currents

As mentioned in Section 6, the impedance measurements for case C charge currents, ie, $D(f) \neq 0$. As denoted in Table 3, a higher frequency, $f = 630$ Hz, is used. The results in Figure 9C show that the validation is in relatively good agreement with the simulation. However, in terms of bias, the deviation between simulation and validation is larger for higher battery temperatures. Moreover, the SD in the validation is also slightly larger than the SD in simulation. Subsequently, this results in a larger MSE in the validation compared with the simulation as shown in Table 3 and Figure 9G. The difference in SD between simulations and measurements, and thus the difference in MSE, could be explained by the fact that the true (dis)charge current is not fully captured by the model for the (dis)charge current in the simulation. Moreover, in the (dis)charge-current model, we only consider the effect of the (dis)charge current on the EIS measurement, ie, the *measurement* artefact. The effect on the electrochemical equilibrium of the battery and thus the effect on the impedance itself are not considered. However, considering the correction for this effect as shown by Zhu et al[32] can be an interesting extension to this work.

Overall, the experimental validation of case C shows that the temperature can be estimated with an accuracy of $\pm1.3°C$ in the presence of (dis)charge currents.

7.4 | Compensating for crosstalk

For this set of measurements, both (dis)charge currents and crosstalk are present. As mentioned in Section 6, the extended models for $\hat{Z}_1$ and $\hat{Z}_2$ (which incorporate crosstalk) have been used for solving (4). The results of the estimation are shown in Figure 9D,H. Overall, bias and SD follow the trend observed in the analysis. Similar to case C, in terms of bias and SD, a deviation is observed between simulation and validation. Therefore, the MSE in Table 3 and Figure 9H of the validation is larger than the MSE in the simulation. The differences between simulation and validation for this case may be due to similar influences as discussed for case C. The results of the experimental validation of this case show that, even when both disturbances are present, the temperature can still be estimated with relatively good accuracy of $\pm1°C$.

7.5 | Discussion

The results of temperature estimation in Figure 9 show that the proposed methods in Table 3, defined by means of finding the smallest MSE in Figure 7, do not necessarily minimise both bias and variance. However, even in the presence of crosstalk interference and (dis)charge currents (ie, case D), the proposed estimation method yields a bias within $\pm1°C$, as shown in Figure 9D. To further improve the method, it is necessary to compensate for the disturbances caused by (dis)charge currents. This would require synchronising the pack-current measurements with the impedance measurements, which is not possible with the experimental setup used in this paper. Still, in theory, this synchronisation could reduce the large MSE seen at lower frequencies in Figure 7 (cases C and D) and would allow the selection of a lower frequency f. This would result in a smaller MSE for the temperature estimation because of the higher sensitivity of the impedance with respect to temperature at lower frequencies. Also, improvements in modelling accuracy, eg, considering the *model* artefact caused by the (dis)charge current (see Section 4), could help to improve the accuracy of the temperature estimation.

Although temperature estimation in case of an unknown SoC can be relatively accurate,[7] it should be noted that the battery SoC is assumed to be known in this paper. However, the SoC is generally not known but estimated by the BMS using model-based estimation algorithms.[35,36] This

will most likely introduce uncertainty on the temperature estimate, and, therefore, it is important to employ a relatively accurate SoC estimation method.[37] Another aspect that needs to be considered for further research is the performance of the estimation method in the presence of temperature gradients across the battery pack[38,39] as well as battery ageing.[25] In particular, if the effect of ageing is not included in the impedance model, the optimal choice for α may not be $\alpha = .5$ as selected in this paper. This has been shown by Beelen,[26,chapter 7] where ageing did occur and predominantly affected the real part of the battery impedance. Therefore, a different value for α, ie, $\alpha = 0$, has been selected in this study in order to achieve satisfactory accuracy of the temperature estimation in the presence of ageing. Alternatively, ageing may also predominantly be present at lower frequencies, affecting the real and imaginary part of the impedance.[8] This may lead to a different choice in excitation frequency, ie, avoiding frequencies at which the impedance may be influenced by the ageing phenomenon. A more interesting approach would be to incorporate a model of the ageing phenomenon in the impedance model so as to include the effect of ageing in the estimation method. Consequently, the selection of α and f will not be based on avoiding the influence of the ageing phenomenon (since it has been captured in the model), allowing for a selection of α and f that yield more accurate temperature estimates (eg, selecting low frequencies and $\alpha = .5$).

Finally, the impedance-based temperature estimation method has been validated experimentally on a two-cell battery pack in this paper to show a proof of concept of the extended method, thereby taking a first step towards development of the method for application on a full-size battery pack of, eg, an electric vehicle. On the basis of the promising estimation results of the estimation method with the two-cell battery pack in this study, future research should therefore focus on developing and testing the method for larger-size battery packs (eg, more than two cells). Moreover, since the goal of this paper was to obtain a proof of concept for extending impedance-based temperature estimation towards its application in battery packs, future research can significantly contribute to develop this method further, eg, through more extensive experimental validation under a wide variety of circumstances.

8 | CONCLUSIONS

In this paper, we have investigated the extension of impedance-based temperature estimation towards its application in battery packs. This has been done by addressing two important challenges that arise when

extending the method: the disturbance caused by (dis)charge currents and crosstalk interference between cells. To address these challenges, firstly, we have extended an existing framework for temperature estimation by including the aforementioned disturbances by modelling these artefacts. As an extension to an existing study,[20] it has been shown that crosstalk neither depends on temperature nor on SoC. Also, it has been shown that (dis)charge currents can be modelled using a deterministic as well as a stochastic approach, where the deterministic approach should be used if the (dis)charge current can be measured synchronously with the impedance measurement. This was not possible with the experimental setup is this paper, prompting the use of the stochastic approach.

Second, we used this extended temperature estimation framework to design an optimal (in the mean-square-error sense) temperature estimation method by analysing the effect of the disturbances on the temperature estimation in combination with the choice of the excitation frequency. Subsequently, using this analysis, an optimal estimation method has been synthesised. Although the battery impedance is most sensitive to temperature at low frequencies, we arrived at a trade-off where a higher frequency is selected, which is less sensitive to temperature, but where the disturbances caused by (dis)charge currents are avoided. Overall, this yields the most accurate temperature estimate. We have found that, even in the presence of both (dis)charge currents and crosstalk interference, the optimal parameters yield good results in terms of an MSE and provide an accuracy of $\pm 1°$C for the temperature estimation. Therefore, on the basis of the experimental results with the two-cell battery pack used in this paper, applicability of impedance-based temperate estimation to real applications with full-size battery packs has come one step closer. Still, further improvements such as (dis)charge current synchronisation or crosstalk mitigation through alternate pack arrangements should be investigated, as well as the application of the method to a full-size battery pack and an extensive validation under a wider range of circumstances and possible applications.

ORCID
Henrik Beelen https://orcid.org/0000-0001-8645-5441
Kartik Mundaragi Shivakumar https://orcid.org/0000-0001-9875-4932

Luc Raijmakers https://orcid.org/0000-0002-7166-8644
M.C.F. Donkers https://orcid.org/0000-0003-1465-5529
Henk Jan Bergveld https://orcid.org/0000-0001-6498-3083

ENDNOTES

[1] Note that synchronising the measurement of current, usually measured in a separate integrated circuit, and cell voltages, usually measured by multiple stacked integrated circuits, is not trivial. It needs to be controlled separately from a central controller using a single serial communication bus, which also severely limits the bandwidth with which the effect of the discharge current could be measured.

[2] In the presence of (dis)charge currents, the induced voltage $V_n(f)$ depends not only on the measurement current $I_n(f)$ of the SCS but also on the (dis)charge current $D(f)$. If $D(f)$ is known exactly, the impedance of cell n can be obtained through $Z_n(f) = \frac{V_n(f)}{I_n(f)+D(f)}$.

[3] The assumption that $D(f)$ is zero-mean is based on the fact that we assume that the current-voltage relation of the battery is linear, which means that the DC-component of $d(t)$ (not to be confused with the DC-component of the stimulus for impedance measurements), which corresponds to $f = 0$ of the Fourier transform signal $D(f)$, will not influence the EIS measurement at the typical frequencies under consideration. Since the current-voltage relation is generally nonlinear, the DC-component of $d(t)$ could influence the EIS measurements. How to deal with this during EIS measurements is still an open and important topic for further research. However, in case of a large battery pack, for example, for an electric vehicle, the DC-component of $d(t)$ is relatively small with respect to the battery capacity and in that case, as shown by Raijmakers et al.,[9] impedance-based temperature estimation can still be applied. Therefore, we assume $D(f)$ to be zero-mean.

REFERENCES

1. Rahimi-Eichi H, Ojha U, Baronti F, Chow M. Battery management system: an overview of its application in the smart grid and electric vehicles. *IEEE Industrial Electronics Magazine*. 2013;7(2):4-16.

2. Hannan MA, Lipu MSH, Hussain A, Mohamed A. A review of lithium-ion battery state of charge estimation and management system in electric vehicle applications: challenges and recommendations. *Renew Sustain Energy Rev*. 2017;78:834-854.

3. Wang Y, Gao Q, Wang G, Lu P, Zhao M, Bao W. A review on research status and key technologies of battery thermal management and its enhanced safety. *International Journal of Energy Research*. 2018;42(13):4008-4033.

4. Raijmakers LHJ, Danilov DL, Eichel R-A, Notten PHL. A review on various temperature-indication methods for Li-ion batteries. *Appl Energy*. 2019;240:918-945.

5. Barsoukov E, Macdonald JR. *Impedance Spectroscopy Theory, Experiment, and Applications*. 2nd ed. John Wiley & Sons; 2005.

6. Wei X, Wang X, Dai H. Practical on-board measurement of lithium ion battery impedance based on distributed voltage and current sampling. *Energies*. 2018;11(1):64.

7. Beelen HPGJ, Raijmakers LHJ, Donkers MCF, Notten PHL, Bergveld HJ. A comparison and accuracy analysis of impedance-based temperature estimation methods for Li-ion batteries. *Appl Energy*. 2016;175:128-140.

8. Raijmakers LHJ, Danilov DL, van Lammeren JPM, Lammers MJG, Notten PHL. Sensorless battery temperature measurements based on electrochemical impedance spectroscopy. *J Power Sources*. 2014;247:539-544.

9. Raijmakers LHJ, Danilov DL, van Lammeren JPM, Lammers MJG, Bergveld HJ, Notten PHL. Non-zero intercept frequency: an accurate method to determine the integral temperature of Li-ion batteries. *IEEE Transactions on Industrial Electronics*. 2016;63(5):3168-3178.

10. Schmidt JP, Arnold S, Loges A, Werner D, Wetzel T, Ivers-Tiffée E. Measurement of the internal cell temperature via impedance: evaluation and application of a new method. *J Power Sources*. 2013;243:110-117.

11. Srinivasan R. Monitoring dynamic thermal behavior of the carbon anode in a lithium-ion cell using a four-probe technique. *J Power Sources*. 2012;198:351-358.

12. Richardson RR, Howey DA. Sensorless battery internal temperature estimation using a Kalman filter with impedance measurement. *IEEE Transactions on Sustainable Energy*. 2015;6(4):1190-1199.

13. Zhu J, Sun Z, Wei X, Dai H. A new lithium-ion battery internal temperature on-line estimate method based on electrochemical impedance spectroscopy measurement. *J Power Sources*. 2015;274:990-1004.

14. Howey DA, Mitcheson PD, Yufit V, Offer G, Brandon NP. On-line measurement of battery impedance using motor controller excitation. *IEEE Transactions on Vehicular Technology*. 2014;63(6):2557-2566.

15. Spinner NS, Love CT, Rose-Pehrsson SL, Tuttle SG. Expanding the operational limits of the single-point impedance diagnostic for internal temperature monitoring of lithium-ion batteries. *Electrochim Acta*. 2015;174:488-493.

16. Koch R, Jossen A. *Temperature Measurement of Large Format Pouch Cells with Impedance Spectroscopy*. Goyang, Korea: In Proc, International Electric Vehicle Symposium and Exhibition; 2015.

17. Raijmakers LHJ. Sensorless temperature measurements for advanced battery management systems. *Dissertation, Delft University of Technology*. 2018.

18. Richardson RR, Ireland PT, Howey DA. Battery internal temperature estimation by combined impedance and surface temperature measurement. *J Power Sources*. 2014;265:254-261.

19. Srinivasan R, Carkhuff BG, Butler MH, Baisden AC. Instantaneous measurement of the internal temperature in lithium-ion rechargeable cells. *Electrochim Acta*. 2011;56:6198-6204.

20. Raijmakers LHJ, Mundaragi Shivakumar K, Donkers MCF, Bergveld HJ. Crosstalk interferences on impedance measurements in battery packs. *Proc. IFAC Symposium on Advances in Automotive Control*; Kolmården, Sweden: Elsevier; 2016:42-47.

21. Orazem ME, Tribollet B. John Wiley & Sons. *Electrochemical Impedance Spectroscopy*. 1st ed. Hoboken, NJ: John Wiley & Sons; 2008.

22. Fleischer C, Waag W, Heyn H-M, Sauer DU. On-line adaptive battery impedance parameter and state estimation considering physical principles in reduced order equivalent circuit battery models: part 1. Requirements, critical review of methods and modeling. *J Power Sources*. 2014;260:276-291.

23. Fleischer C, Waag W, Heyn H-M, Sauer DU. On-line adaptive battery impedance parameter and state estimation considering physical principles in reduced order equivalent circuit battery models: part 2. Parameter and state estimation. *J Power Sources*. 2014;262:457-482.

24. Ranieri M, Alberto D, Piret H, Cattin V. Electronic module for the thermal monitoring of a Li-ion battery cell through the electrochemical impedance estimation. *Microelectronics Reliability*. 2017;79:410-415.

25. Waag W, Käbitz S, Sauer DU. Experimental investigation of the lithium-ion battery impedance characteristic at various conditions and aging states and its influence on the application. *Appl Energy*. 2013;102:885-897.

26. Beelen HPGJ. *Model-Based Temperature and State-of-Charge Estimation for Li-ion Batteries*. Dissertation: Eindhoven University of Technology; 2019.

27. Bergveld HJ, Kruijt WS, Notten PHL. *Battery Management Systems: Design by Modelling*. 1st ed. Eindhoven: Springer Science + Business Media; 2002.

28. Buller S, Thele M, Karden E, De Doncker RW. Impedance-based non-linear dynamic battery modeling for automotive applications. *J Power Sources*. 2003;113(2):422-430.

29. Yates RD, Goodman DJ. *Probability and Stochastic Processes: A Friendly Introduction for Electrical and Computer Engineers*. 2nd ed. Hoboken, NJ: John Wiley & Sons; 2005.

30. Barai A, Chouchelamane GH, Guo Y, Mcgordon A, Jennings P. A study on the impact of lithium-ion cell relaxation on electrochemical impedance spectroscopy. *J Power Sources*. 2015;280: 74-80.

31. Schindler S, Bauer M, Petzl M, Danzer MA. Voltage relaxation and impedance spectroscopy as in-operando methods for the detection of lithium plating on graphitic anodes in commercial lithium-ion cells. *J Power Sources*. 2016;304:170-180.

32. Zhu J, Sun Z, Wei X, Dai H. Battery internal temperature estimation for LiFePO4 battery based on impedance phase shift under operating conditions. *Energies*. 2017;10(1):60.

33. Childers D, Miller S. *Probability and Random Processes*. 1st ed. Cambridge, MA: Academic Press; 2012.

34. Rubinstein RY, Kroese DP. *Simulation and the Monte Carlo Method*. 2nd ed. Hoboken, NJ: John Wiley & Sons; 2008.

35. Yang F, Xing Y, Wang D, Tsui KL. A comparative study of three model-based algorithms for estimating state-of-charge of lithium-ion batteries under a new combined dynamic loading profile. *Appl Energy*. 2016;164:387-399.

36. Campestrini C, Heil T, Kosch S, Jossen A. A comparative study and review of different Kalman filters by applying an enhanced validation method. *Journal of Energy Storage*. 2016;8:142-159.

37. Barillas JK, Li J, Günther C, Danzer MA. A comparative study and validation of state estimation algorithms for Li-ion batteries in battery management systems. *Appl Energy*. 2015;155:455-462.

38. Klein M, Tong S, Park JW. In-plane nonuniform temperature effects on the performance of a large-format lithium-ion pouch cell. *Appl Energy*. 2016;165:639-647.

39. Dai H, Jiang B, Wei X. Impedance characterization and modeling of lithium-ion batteries considering the internal temperature gradient. *Energies*. 2018;11(1):220.